

Proceedings of the 12th International Conference on
Computational Fluid Dynamics in the Oil & Gas,
Metallurgical and Process Industries

Progress in Applied CFD – CFD2017



SINTEF Proceedings

Editors:

Jan Erik Olsen and Stein Tore Johansen

Progress in Applied CFD – CFD2017

Proceedings of the 12th International Conference on Computational Fluid Dynamics
in the Oil & Gas, Metallurgical and Process Industries

SINTEF Academic Press

SINTEF Proceedings no 2

Editors: Jan Erik Olsen and Stein Tore Johansen

Progress in Applied CFD – CFD2017

Selected papers from 10th International Conference on Computational Fluid Dynamics in the Oil & Gas, Metallurgical and Process Industries

Key words:

CFD, Flow, Modelling

Cover, illustration: Arun Kamath

ISSN 2387-4295 (online)

ISBN 978-82-536-1544-8 (pdf)

© Copyright SINTEF Academic Press 2017

The material in this publication is covered by the provisions of the Norwegian Copyright Act. Without any special agreement with SINTEF Academic Press, any copying and making available of the material is only allowed to the extent that this is permitted by law or allowed through an agreement with Kopinor, the Reproduction Rights Organisation for Norway. Any use contrary to legislation or an agreement may lead to a liability for damages and confiscation, and may be punished by fines or imprisonment

SINTEF Academic Press

Address: Forskningsveien 3 B
 PO Box 124 Blindern
 N-0314 OSLO

Tel: +47 73 59 30 00

Fax: +47 22 96 55 08

www.sintef.no/byggforsk

www.sintefbok.no

SINTEF Proceedings

SINTEF Proceedings is a serial publication for peer-reviewed conference proceedings on a variety of scientific topics.

The processes of peer-reviewing of papers published in SINTEF Proceedings are administered by the conference organizers and proceedings editors. Detailed procedures will vary according to custom and practice in each scientific community.

PREFACE

This book contains all manuscripts approved by the reviewers and the organizing committee of the 12th International Conference on Computational Fluid Dynamics in the Oil & Gas, Metallurgical and Process Industries. The conference was hosted by SINTEF in Trondheim in May/June 2017 and is also known as CFD2017 for short. The conference series was initiated by CSIRO and Phil Schwarz in 1997. So far the conference has been alternating between CSIRO in Melbourne and SINTEF in Trondheim. The conferences focuses on the application of CFD in the oil and gas industries, metal production, mineral processing, power generation, chemicals and other process industries. In addition pragmatic modelling concepts and bio-mechanical applications have become an important part of the conference. The papers in this book demonstrate the current progress in applied CFD.

The conference papers undergo a review process involving two experts. Only papers accepted by the reviewers are included in the proceedings. 108 contributions were presented at the conference together with six keynote presentations. A majority of these contributions are presented by their manuscript in this collection (a few were granted to present without an accompanying manuscript).

The organizing committee would like to thank everyone who has helped with review of manuscripts, all those who helped to promote the conference and all authors who have submitted scientific contributions. We are also grateful for the support from the conference sponsors: ANSYS, SFI Metal Production and NanoSim.

Stein Tore Johansen & Jan Erik Olsen



Organizing committee:

Conference chairman: Prof. Stein Tore Johansen

Conference coordinator: Dr. Jan Erik Olsen

Dr. Bernhard Müller

Dr. Sigrid Karstad Dahl

Dr. Shahriar Amini

Dr. Ernst Meese

Dr. Josip Zoric

Dr. Jannike Solsvik

Dr. Peter Witt

Scientific committee:

Stein Tore Johansen, SINTEF/NTNU

Bernhard Müller, NTNU

Phil Schwarz, CSIRO

Akio Tomiyama, Kobe University

Hans Kuipers, Eindhoven University of Technology

Jinghai Li, Chinese Academy of Science

Markus Braun, Ansys

Simon Lo, CD-adapco

Patrick Segers, Universiteit Gent

Jiyuan Tu, RMIT

Jos Derksen, University of Aberdeen

Dmitry Eskin, Schlumberger-Doll Research

Pär Jönsson, KTH

Stefan Pirker, Johannes Kepler University

Josip Zoric, SINTEF

CONTENTS

PRAGMATIC MODELLING	9
On pragmatism in industrial modeling. Part III: Application to operational drilling	11
CFD modeling of dynamic emulsion stability	23
Modelling of interaction between turbines and terrain wakes using pragmatic approach	29
FLUIDIZED BED	37
Simulation of chemical looping combustion process in a double looping fluidized bed reactor with cu-based oxygen carriers.....	39
Extremely fast simulations of heat transfer in fluidized beds.....	47
Mass transfer phenomena in fluidized beds with horizontally immersed membranes	53
A Two-Fluid model study of hydrogen production via water gas shift in fluidized bed membrane reactors	63
Effect of lift force on dense gas-fluidized beds of non-spherical particles	71
Experimental and numerical investigation of a bubbling dense gas-solid fluidized bed	81
Direct numerical simulation of the effective drag in gas-liquid-solid systems	89
A Lagrangian-Eulerian hybrid model for the simulation of direct reduction of iron ore in fluidized beds.....	97
High temperature fluidization - influence of inter-particle forces on fluidization behavior	107
Verification of filtered two fluid models for reactive gas-solid flows	115
BIOMECHANICS.....	123
A computational framework involving CFD and data mining tools for analyzing disease in carotid artery	125
Investigating the numerical parameter space for a stenosed patient-specific internal carotid artery model.....	133
Velocity profiles in a 2D model of the left ventricular outflow tract, pathological case study using PIV and CFD modeling.....	139
Oscillatory flow and mass transport in a coronary artery.....	147
Patient specific numerical simulation of flow in the human upper airways for assessing the effect of nasal surgery.....	153
CFD simulations of turbulent flow in the human upper airways	163
OIL & GAS APPLICATIONS	169
Estimation of flow rates and parameters in two-phase stratified and slug flow by an ensemble Kalman filter	171
Direct numerical simulation of proppant transport in a narrow channel for hydraulic fracturing application	179
Multiphase direct numerical simulations (DNS) of oil-water flows through homogeneous porous rocks	185
CFD erosion modelling of blind tees	191
Shape factors inclusion in a one-dimensional, transient two-fluid model for stratified and slug flow simulations in pipes	201
Gas-liquid two-phase flow behavior in terrain-inclined pipelines for wet natural gas transportation	207

NUMERICS, METHODS & CODE DEVELOPMENT	213
Innovative computing for industrially-relevant multiphase flows	215
Development of GPU parallel multiphase flow solver for turbulent slurry flows in cyclone.....	223
Immersed boundary method for the compressible Navier–Stokes equations using high order summation-by-parts difference operators	233
Direct numerical simulation of coupled heat and mass transfer in fluid-solid systems	243
A simulation concept for generic simulation of multi-material flow, using staggered Cartesian grids.....	253
A cartesian cut-cell method, based on formal volume averaging of mass, momentum equations.....	265
SOFT: a framework for semantic interoperability of scientific software	273
 POPULATION BALANCE	 279
Combined multifluid-population balance method for polydisperse multiphase flows	281
A multifluid-PBE model for a slurry bubble column with bubble size dependent velocity, weight fractions and temperature.....	285
CFD simulation of the droplet size distribution of liquid-liquid emulsions in stirred tank reactors	295
Towards a CFD model for boiling flows: validation of QMOM predictions with TOPFLOW experiments	301
Numerical simulations of turbulent liquid-liquid dispersions with quadrature-based moment methods.....	309
Simulation of dispersion of immiscible fluids in a turbulent couette flow	317
Simulation of gas-liquid flows in separators - a Lagrangian approach.....	325
CFD modelling to predict mass transfer in pulsed sieve plate extraction columns	335
 BREAKUP & COALESCENCE	 343
Experimental and numerical study on single droplet breakage in turbulent flow	345
Improved collision modelling for liquid metal droplets in a copper slag cleaning process	355
Modelling of bubble dynamics in slag during its hot stage engineering.....	365
Controlled coalescence with local front reconstruction method	373
 BUBBLY FLOWS	 381
Modelling of fluid dynamics, mass transfer and chemical reaction in bubbly flows	383
Stochastic DSMC model for large scale dense bubbly flows.....	391
On the surfacing mechanism of bubble plumes from subsea gas release.....	399
Bubble generated turbulence in two fluid simulation of bubbly flow	405
 HEAT TRANSFER	 413
CFD-simulation of boiling in a heated pipe including flow pattern transitions using a multi-field concept	415
The pear-shaped fate of an ice melting front	423
Flow dynamics studies for flexible operation of continuous casters (flow flex cc).....	431
An Euler-Euler model for gas-liquid flows in a coil wound heat exchanger.....	441
 NON-NEWTONIAN FLOWS.....	 449
Viscoelastic flow simulations in disordered porous media	451
Tire rubber extrudate swell simulation and verification with experiments	459
Front-tracking simulations of bubbles rising in non-Newtonian fluids.....	469
A 2D sediment bed morphodynamics model for turbulent, non-Newtonian, particle-loaded flows.....	479

METALLURGICAL APPLICATIONS.....	491
Experimental modelling of metallurgical processes	493
State of the art: macroscopic modelling approaches for the description of multiphysics phenomena within the electroslag remelting process	499
LES-VOF simulation of turbulent interfacial flow in the continuous casting mold	507
CFD-DEM modelling of blast furnace tapping	515
Multiphase flow modelling of furnace tapholes	521
Numerical predictions of the shape and size of the raceway zone in a blast furnace.....	531
Modelling and measurements in the aluminium industry - Where are the obstacles?	541
Modelling of chemical reactions in metallurgical processes.....	549
Using CFD analysis to optimise top submerged lance furnace geometries	555
Numerical analysis of the temperature distribution in a martensic stainless steel strip during hardening.....	565
Validation of a rapid slag viscosity measurement by CFD.....	575
Solidification modeling with user defined function in ANSYS Fluent.....	583
Cleaning of polycyclic aromatic hydrocarbons (PAH) obtained from ferroalloys plant.....	587
Granular flow described by fictitious fluids: a suitable methodology for process simulations	593
A multiscale numerical approach of the dripping slag in the coke bed zone of a pilot scale Si-Mn furnace.....	599
 INDUSTRIAL APPLICATIONS	 605
Use of CFD as a design tool for a phosphoric acid plant cooling pond	607
Numerical evaluation of co-firing solid recovered fuel with petroleum coke in a cement rotary kiln: Influence of fuel moisture	613
Experimental and CFD investigation of fractal distributor on a novel plate and frame ion-exchanger	621
 COMBUSTION	 631
CFD modeling of a commercial-size circle-draft biomass gasifier.....	633
Numerical study of coal particle gasification up to Reynolds numbers of 1000.....	641
Modelling combustion of pulverized coal and alternative carbon materials in the blast furnace raceway	647
Combustion chamber scaling for energy recovery from furnace process gas: waste to value	657
 PACKED BED.....	 665
Comparison of particle-resolved direct numerical simulation and 1D modelling of catalytic reactions in a packed bed	667
Numerical investigation of particle types influence on packed bed adsorber behaviour	675
CFD based study of dense medium drum separation processes	683
A multi-domain 1D particle-reactor model for packed bed reactor applications.....	689
 SPECIES TRANSPORT & INTERFACES	 699
Modelling and numerical simulation of surface active species transport - reaction in welding processes	701
Multiscale approach to fully resolved boundary layers using adaptive grids.....	709
Implementation, demonstration and validation of a user-defined wall function for direct precipitation fouling in Ansys Fluent.....	717

FREE SURFACE FLOW & WAVES	727
Unresolved CFD-DEM in environmental engineering: submarine slope stability and other applications.....	729
Influence of the upstream cylinder and wave breaking point on the breaking wave forces on the downstream cylinder	735
Recent developments for the computation of the necessary submergence of pump intakes with free surfaces	743
Parallel multiphase flow software for solving the Navier-Stokes equations	752
 PARTICLE METHODS	 759
A numerical approach to model aggregate restructuring in shear flow using DEM in Lattice-Boltzmann simulations	761
Adaptive coarse-graining for large-scale DEM simulations.....	773
Novel efficient hybrid-DEM collision integration scheme.....	779
Implementing the kinetic theory of granular flows into the Lagrangian dense discrete phase model.....	785
Importance of the different fluid forces on particle dispersion in fluid phase resonance mixers	791
Large scale modelling of bubble formation and growth in a supersaturated liquid.....	798
 FUNDAMENTAL FLUID DYNAMICS	 807
Flow past a yawed cylinder of finite length using a fictitious domain method	809
A numerical evaluation of the effect of the electro-magnetic force on bubble flow in aluminium smelting process.....	819
A DNS study of droplet spreading and penetration on a porous medium.....	825
From linear to nonlinear: Transient growth in confined magnetohydrodynamic flows.....	831

CFD SIMULATION OF THE DROPLET SIZE DISTRIBUTION OF LIQUID-LIQUID EMULSIONS IN STIRRED TANK REACTORS

Reza FARZAD¹, Simon SCHNEIDERBAUER^{1,2}

¹ Christian Doppler Laboratory for Multi-Scale Modelling of Multiphase Processes, Johannes Kepler University, 4040 Linz, AUSTRIA

² Department of Particulate Flow Modelling, Johannes Kepler University, 4040 Linz, AUSTRIA

* E-mail: reza.farzad@jku.at

ABSTRACT

Predicting the drop size distribution (DSD) is essential in particulate flows such as emulsions as it affects mass transfer and heat transfer. In the current work we developed a novel numerical method to account for droplet breakup. The droplet breakup relies on an in-house developed correlation which depends on the local shear rate and some fluid properties. Commonly, a population balance equation (PBE) is employed to describe the breakup and coalescence of the droplets; however, such an approach does commonly not distinguish between different slip velocities of the smaller and larger droplets. Therefore, we propose a hybrid modelling strategy, which combines an Eulerian-Eulerian two-fluid model (TFM) and a Lagrangian discrete particle model (DPM), which is referred to as the Hybrid TFM-DPM model. This method enables the efficient evaluation of the poly-disperse liquid-liquid drag force from the local distribution of the different droplet diameters. The latter can be obtained by tracking statistically representative droplet trajectories for each droplet diameter class. Finally, we applied this novel approach to a liquid-liquid emulsion in a stirred tank presented. The results clearly show that the present method is able to predict the droplet size distribution for different rotational speeds of the stirrer.

Keywords: Emulsion, Droplet breakup, Coalescence, Hybrid TFM-DPM

NOMENCLATURE

Notation

We Weber number, [-].

Re Reynolds number, [-].

A Dimensionless constant, [-].

a Shear rate, [-].

D_{32} Sauter mean diameter, [m].

D_{90} 90% of the droplets are smaller than this value, [m].

F_k^{poly} Drag force acting on a parcel with d_k , [kg·m/s²].

g Gravity acceleration, [m/s²].

h Characteristic length, [m].

K Interphase momentum exchange coefficient

L Impeller diameter of stirred tank (Characteristic length), [m].

\vec{u} Velocity field, [m/s].

\tilde{u} Average velocity, [m/s].

Greek Symbols

ρ Mass density, [kg/m³].

μ Dynamic viscosity, [kg/m·s].

γ Interfacial tension, [kg/s²].

ε Turbulence dissipation rate. [m²/s³].

ζ Collision frequency, [#s].

λ Coalescence efficiency, [-].

Γ Coalescence frequency, [#s].

τ Shear stress, [kg/m·s²].

$\tau_{col,d}$ Collisional time scale.

ϕ Dispersed phase volume fraction. [-]

Sub/superscripts

c Continuous phase.

d Dispersed phase.

k Index of parcel.

p Parcel.

INTRODUCTION

Emulsions are widely used in the several industries such as food, pharmaceutical, cosmetic, chemical and petroleum. Drop size distribution (DSD) plays the key role as it controls mass transfer and heat transfer of the liquid-liquid system inside the reactor (Leng and Calabrese, 2004). Wide range of studies are done both numerically and experimentally to cover the DSD issues in the stirred tank reactor. There are several experimental studies focus on the single drop breakup experiment in order to define the breakup kernel for the Population balance equation (PBE) (Maaß et al., 2012; Solsvik et al., 2014; Solsvik and Jakobsen, 2015) and some others

investigated DSD regardless of the events happening to each droplet (Boxall et al., 2010; Calabrese et al., 1986; Coualaloglou and Tavlarides, 1977, 1976; Narsimhan et al., 1980; Ohtake et al., 1987; Wang and Calabrese, 1986). In addition, there are some additional studies, where computational fluid dynamic (CFD) in combination with PBE modelling is performed to predict the PSD of liquid-liquid emulsions (Agterof et al., 2003; Roudsari et al., 2012).

PBE is commonly used to take account for the break up and coalescence of the droplets, although it is computationally not affordable to consider the different slip velocities of the different droplet sizes. Furthermore, the PBE requires kernels for breakup and coalescence, which are difficult to obtain due to finding the parameters such as the breakage frequency (Ramkrishna, 2000). In the current work, a hybrid approach is proposed, which combines the Eulerian-Eulerian two fluid model (TFM) and the Lagrangian discrete particle model (DPM) (Schneiderbauer et al., 2016a, 2016b). Here, the breakup of the droplets can be evaluated based on individual representative droplets. Moreover, hybrid TFM-DPM strategy has the advantage to acquire the Sauter mean diameter from DPM side (Lagrangian) and deliver it to TFM in order to calculate the accurate interphase momentum exchange term (Schneiderbauer et al., 2015). However, this hybrid approach requires the local equilibrium droplet size distribution. In the literature there are correlations, which evaluate the global Sauter mean diameter in a stirred tank reactors. The early stage correlation was developed based on the Kolmogorov length scale (Kolmogorov, 1941) by the work of Shinnar and Church (Shinnar and Church, 1960) and Chen and Middleman (Chen and Middleman, 1967) which reads,

$$\frac{D_{32}}{L} = AWe^{-0.6} \quad (1)$$

There are similar works available, which give different correlations for the global Sauter mean diameter (Calabrese et al., 1986; Coualaloglou and Tavlarides, 1976; Wang and Calabrese, 1986). However, there is no available local correlation for Sauter mean diameter based on the local fluid dynamic parameters (such as turbulence dissipation rate, ϵ) as it is difficult to obtain. Therefore, we investigated the droplet breakup in a Taylor-couette flow, in which the measurement of fluid dynamic parameters such as shear rate is well defined (Farzad et al., 2016). The resulting correlation depends on the shear rate and the fluid physical properties like density, viscosity and interfacial tension which is written as below (Farzad et al., 2016),

$$\frac{D_{32}}{h} = We^{-\frac{1}{6}} Re^{-\frac{1}{4}} \left(\frac{\mu_d}{\mu_c} \right)^{0.33} \left(\frac{\rho_d}{\rho_c} \right)^{-6.6} \quad (2)$$

$$We = \frac{\rho_c a^2 h^3}{\gamma} \quad Re = \frac{\rho_c a h^2}{\mu_c}$$

Note that, the power of h becomes zero due to combination of the h, Weber number and Reynolds

number. Therefore, the normalized Sauter mean diameter is independent of the characteristic length (h). Finally, while the modelling of breakup can be efficiently realized on a droplet level, the coalescence of the droplets would require resolving the collisions between individual droplets. In the following, we present novel models for breakup and coalescence. On the one hand, the breakup model is connected to equation (2) and on the other hand, the coalescence model represents a different discretization strategy of the population balance equations.

DROPLET BREAKUP MODEL

The present breakup model depends on the local Sauter mean diameter (equation 2), which can be obtained by using the local shear rate and the system's physical properties. Furthermore, our in-house experimental data (Farzad et al., 2016) reveals that the standard deviation scales linearly with the Sauter mean diameter, i.e. $\sigma = 0.33D_{32}$, and that the DSD follows a log-normal distribution; this observation is also consistent with literature (Boxall et al., 2010). Therefore, the full local equilibrium DSD can be determined by using the Sauter mean diameter from the correlation (equation 2) and $\sigma = 0.33D_{32}$. Thus, if a droplet is much larger than the the mean droplet size given from the DSD it might be prone to breakup. In this work, we employ the D_{90} for this threshold, which can be computed in each computational cell from the corresponding local DSD (Figure 1). If a droplet is larger D_{90} we sample a random number following the log-normal distribution. Only if this random number is larger than D_{90} as well, the droplet will break into two daughter droplets, where the diameter of the first daughter droplet is given by a second random number following the log-normal distribution. Note that, based on our assumption the local droplets (parcels) which are smaller than D_{90} remain stable as they are inside the local size distribution. Therefore, the local size distribution is constant and global size distribution changes till it reaches a steady state. Consequently, the diameter of the second daughter droplet can be easily computed from the volumes of the mother droplet and the first daughter droplet. This model was implemented as a user-defined function (UDF) to be used in the ANSYS FLUENT. The numerical implementation scheme will be discussed later. Note that breakup is not resolved for each droplet as it computationally costly and in most of the cases impossible; therefore, DPM uses parcels instead of particles which represent a group of particles with the identical diameter to reduce the computational costs.

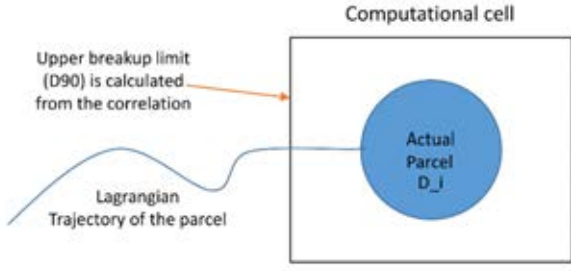


Figure 1: Schematic view of Lagrangian parcel which enters a specific computational cell with an upper breakup limit. If the parcel is larger than the limit then it breaks; otherwise, it remains unchanged.

DROPLET COALESCENCE MODEL

Modelling coalescence is more demanding compared to the breakup. Coalescence can be thought as the combination of collision frequency $\zeta(d, d')$ and coalescence efficiency $\lambda(d, d')$. Thus, a general form of the coalescence frequency reads (Coulaloglou and Tavlarides, 1977; Leng and Calabrese, 2004),

$$\Gamma(d, d') = \zeta(d, d')\lambda(d, d') \quad (3)$$

Computing the collision frequency directly from droplet interactions is computationally very demanding and would decline the benefits of the hybrid approach. Therefore, we follow Coulaloglou and Tavlarides (Coulaloglou and Tavlarides, 1977), who defined the collision frequency and coalescence efficiency as below:

$$\zeta(d, d') = c_1 \frac{\varepsilon^{1/3}}{1 + \phi} (d + d')^2 (d^{2/3} + d'^{2/3})^{1/2} \quad (4)$$

$$\lambda(d, d') = \exp(-c_2 \frac{\mu_c \rho_c \varepsilon}{\sigma^2 (1 + \phi)^3} (\frac{d \cdot d'}{d + d'})^4) \quad (5)$$

Coalescence may occur when at least two droplets collide with each other; however, as noted above computing Γ from the interactions of the Lagrangian parcels would considerably decrease the computational efficiency of the present model. Thus, a different strategy is required to compute the rate of coalescence for the actual Lagrangian parcel. This strategy is outlined in the following: First, similar to PBE modelling we introduce a specific number of diameter classes. For each of this diameter classes, we are able to compute the corresponding volume fraction from mapping the data coming from the Lagrangian parcels to the Eulerian grid used for the TFM solution. Second, based on these “imaginary coalescence partners” given from this binning, we are able to compute the individual rates of coalescence (equation (3)). Note that the representative diameter of each bin is given by its mid diameter. Therefore, if we have N parcels and M bins in a cell, there are $M \times N$ combinations (e.g. $N \approx 2 \times 10^6$ $M = 13$). Third, the amount of volume created due to coalescence is locally stored regarding to its new diameter class in the appropriate diameter bins. Note that all the coalescence which can produce droplets larger than local D_{90} were neglected in order to reduce the computational cost as they are prone to breakup again in the next time step.

After storing the volume of the created droplets, they should be off loaded correctly into the available parcels with appropriate diameter. The volume remains stored until an appropriate parcel enters the computational cell; this procedure is known as “Bus stop model” (Schellander et al., 2012). Bus stop model helps to reduce the computational cost since always injecting the coalescence volume as a new parcel increases the computation time. However, there might be no suitable parcel available (regarding to its diameter class) in the surrounding; then, a new parcel should be injected in the next time step (flow time).

Two-fluid Model (TFM)

Resolving the motion of all droplets are computationally costly; therefore, it is more realistic to consider the averaged equation of motion and treat them as an Eulerian phase (Crowe et al., 2011). Continuity and momentum equations for the dispersed phase read (Ranade, 2001),

Continuity equation

$$\frac{\partial}{\partial t} (\alpha_d \rho_d) + \nabla \cdot (\alpha_d \rho_d \bar{u}_d) = 0 \quad (6)$$

Momentum equation

$$\frac{\partial}{\partial t} (\alpha_d \rho_d \bar{u}_d) + \nabla \cdot (\alpha_d \rho_d \bar{u}_d \bar{u}_d) = -\alpha_d \nabla p + \nabla \cdot (\alpha_d \tau_d) + F_d + \alpha_d \rho_d g \quad (7)$$

F_d which denotes the interphase momentum exchange between the dispersed phase and the continuous phase reads,

$$F_d = K_{cd} (\bar{u}_c - \bar{u}_d) \quad (8)$$

In reality most of the dispersed multiphase flows such as droplets and particles are poly-disperse; therefore, Sauter mean diameter is required to calculate the interphase momentum exchange properly (Schneiderbauer et al., 2015).

Continuity and momentum equations for the continuous phase in a similar manner. This Eulerian-Eulerian approach is also known as TFM.

Discrete phase model (DPM)

This model provides the movement of a single or a cluster of particles (parcel) and tracks them in the flow field. Tracking the parcel trajectories gives the Lagrangian information. The momentum equation for the parcel trajectory is,

$$\frac{\partial}{\partial t} (u_{p,k}) = F_k^{poly} + g \quad (7)$$

Hybrid model

Combining Lagrangian and Eulerian models yields the hybrid model. The TFM model predicts the flow field by

solving the Navier-Stokes equation and the DPM model passes the extra information (e.g. Sauter mean diameter) to the TFM part in order to improve the accuracy of the Eulerian part (Schneiderbauer et al., 2015). Furthermore, sensitivity analysis on several numerical settings reveals that the hybrid model is reliable (Schneiderbauer et al., 2016b).

This model is able to calculate the local Sauter mean diameter which changes the poly-disperse drag force (Figure 2). The modified Lagrangian trajectory can be written as below (Schneiderbauer et al., 2016a),

$$\frac{\partial}{\partial t}(u_{p,k}) = -\frac{1}{\tau_{col,d}}(u_{p,k} - \tilde{u}_d) + F_k^{poly} + g \quad (7)$$



Figure 2: Single Lagrangian parcel trajectory (left side), the continuous droplets travels with local average velocity (middle), hybrid model in which consider the impact of the other existing droplets on the Lagrangian trajectory (right side)

RESULTS AND DISCUSSION

The numerical work by Roudsari et al. (Roudsari et al., 2012) and the experimental data by Boxall et al. (Boxall et al., 2010) were used to validate the proposed models. These works are similar; however, the first one (Roudsari et al., 2012) explains the CFD simulation of the water-in-oil emulsion in stirred tank by applying PBE and validating their results by the second paper (Boxall et al., 2010) which contains the experimental data. The so called Conroe oil was used as the continuous phase and distilled water as the dispersed phase (Boxall et al., 2010). The Conroe oil density, viscosity and interfacial tensions are 842 kg/m³, 3.1 cP and 20 mN/m, respectively. The same geometry was used as Roudsari et al. (Roudsari et al., 2012). However, they used multiple reference frame (MRF) to simulate the impeller's rotation and ran the simulation in steady state but in the current work, dynamic simulation in combination with sliding mesh (SM) was carried out. Hexahedral mesh (Figure 3) of stirred tank reactor (Rushton turbine 6 blades and 4 baffles) was generated by using ANSYS ICEM (260,000 cells).

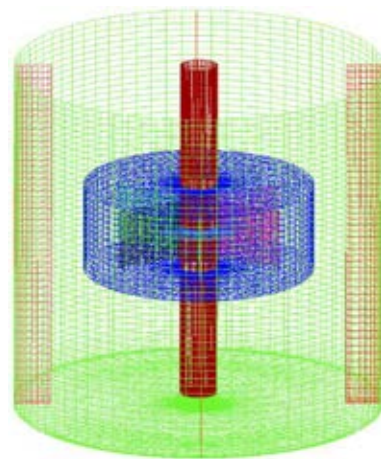


Figure 3: Stirred tank reactor mesh

As noted above, the Sauter mean diameter correlation, the breakup and the coalescence models were implemented as a UDF. The simulation of liquid-liquid system in stirred tank reactor including the hybrid TFM-DPM in combination with k-ε turbulence model was carried out by ANSYS FLUENT 16.2. The time step size was 0.01s.

Breakup

The correlation of Sauter mean diameter (equation 2) was determined based on the dilute oil-water system (dispersed phase volume fraction was 1%) (Farzad et al., 2016); however, the volume fraction of dispersed phase in the experimental work of Boxall et al. (Boxall et al., 2010) is 15% and it can increase the Sauter mean diameter of the droplets due to coalescence (Coulaloglou and Tavlarides, 1976). Therefore, a linear correction factor was defined in the UDF based on the local volume fraction of the secondary phase in order to modify the correlation (equation 2) (Coulaloglou and Tavlarides, 1976).

$$D'_{32} = (1 + n\phi) D_{32}, \quad (8)$$

where n is set to 6.5. Simulation was ran for two rotational speeds, 300 RPM and 600 RPM. The initial droplets with diameter of 0.6 mm and 0.3 mm were injected at t=0 for the 300 RPM (Figure 4) and the 600 RPM (Figure 5) cases, respectively.

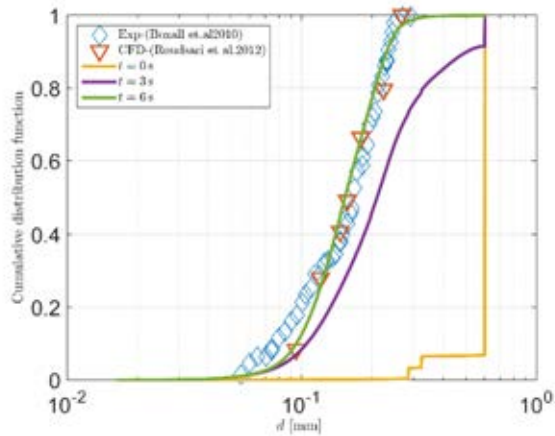


Figure 4: Cumulative drop size distribution at 300 RPM -Water in Conroe oil - Curves show the DSD (simulated) at t=0, 3 and 6 second- shaped scattered experimental data are taken from Boxall et al. (Boxall et al., 2010)- Nabla shaped points are CFD simulation results taken from Roudsari et al. (Roudsari et al., 2012)

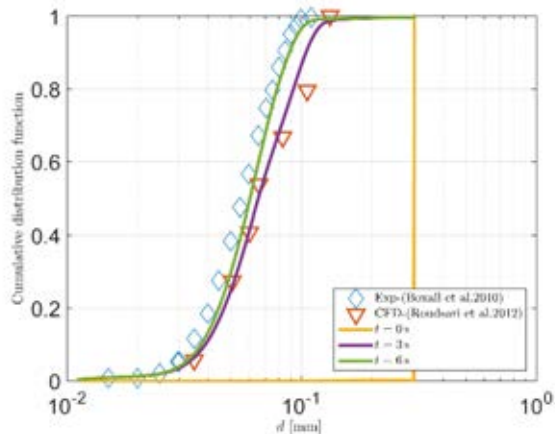


Figure 5: Cumulative drop size distribution at 600 RPM -Water in Conroe oil - Curves show the DSD (simulated) at t=0, 3 and 6 second-Diamond shaped scattered experimental data are taken from Boxall et al. (Boxall et al., 2010)- Nabla shaped points are CFD simulation results taken from Roudsari et al. (Roudsari et al., 2012)

As it can be seen from figure 4 and 5, the final status of the simulated results are in a good agreement with the experimental data (Boxall et al., 2010). Comparing the figures at t=3s (real flow time) reveals that the simulation at 600 RPM reached faster to its final state is compared to the 300 RPM. Therefore, mixing process is happening faster at 600 RPM in comparison with 300 RPM. However, studying the mixing time is not in the scope of this work. In addition, simulated DSD at 600 RPM follows the experimental data (Boxall et al., 2010) more accurately than compared to the simulated data provided by Roudsari et al. (Roudsari et al., 2012). Furthermore, using Lagrangian tracer trajectories provides the possibility to distribute the final simulated results into a large number of bins (400) in order to get smooth DSD. Roudsari et al. (Roudsari et al., 2012) used 7 bins as a part of PBE model available on the ANSYS FLUENT; therefore, their results are not as smooth as the results in the current work.

Coalescence

In order to validate the coalescence model, we study a process dominated by droplet coalescence. For example, when reducing the rotational speed was reduced from 600 RPM to 300 RPM breakup becomes negligible compared to coalescence. Nevertheless, both the breakup and the coalescence models were involved in this part of the simulation. The constant values of collision frequency, $c_1 = 1.29e^{-5}$ and coalescence efficiency, $c_2 = 7.32e^{12}$ were selected from (Maaß et al., 2007). However, the constant for the collision frequency was increased to $c_1 = 1$, in order to speed up the simulation to obtain the preliminary results. Figure 6 illustrates initial results of the coalescence model, where the curve at t=0 is the DSD at 600 RPM and after 0.5s (real flow time) DSD is almost close the experimental data at 300 RPM (Boxall et al., 2010).

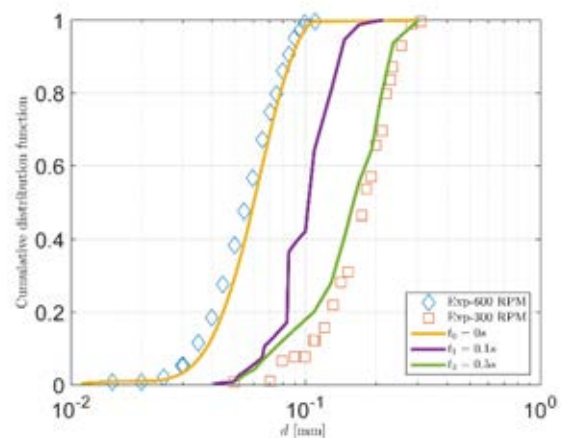


Figure 6: Cumulative drop size distribution evolves by time from 600 RPM to 300 RPM due to coalescence -Water in Crone oil - Curves show the DSD (simulated) at t=0, 0.1 and 0.5 second-Diamond shaped and square shaped scattered experimental data are taken from Boxall et al. (Boxall et al., 2010)

CONCLUSION

In this work, we presented novel breakup and coalescence models for liquid-liquid emulsions in combination with and Eulerian-Lagrangian Hybrid model. The main advantage compared to state of the art PBE modelling approaches is the Lagrangian nature of our approach, which allows the simple evaluation of, for example, residence time distribution.

The breakup model is based on an in-house correlation for Sauter mean diameter (Farzad et al., 2016), while the coalescence model is based on literature correlations. These models were combined with a hybrid TFM-DPM strategy, which allows the efficient analysis of poly-disperse systems. Final results for breakup show that the breakup model works fairly well for the validation case (Boxall et al., 2010; Roudsari et al., 2012). The initial results for the coalescence model are in a good agreement with the experiment (Boxall et al., 2010). However, these models, especially the model for coalescence require further investigation and more validation cases. Especially, larger systems will be subject to future investigations.

REFERENCES

- Agterof, W.G.M., Vaessen, G.E.J., Haagh, G.A.A. V., Klahn, J.K., Janssen, J.J.M., 2003. Prediction of emulsion particle sizes using a computational fluid dynamics approach. *Colloids Surfaces B Biointerfaces* 31, 141–148. doi:10.1016/S0927-7765(03)00051-1
- Boxall, J.A., Koh, C.A., Sloan, E.D., Sum, A.K., Wu, D.T., 2010. Measurement and Calibration of Droplet Size Distributions in Water-in-Oil Emulsions by Particle Video Microscope and a Focused Beam Reflectance Method. *Ind. Eng. Chem. Res.* 49, 1412–1418. doi:10.1021/ie901228e
- Calabrese, R. V., Chang, T.P.K., Dang, P.T., 1986. Drop breakup in turbulent stirred tank contactors. Part I: Effect of dispersed phase viscosity. *AIChE J.* 32, 657–666. doi:10.1002/aic.690320416
- Chen, H.T., Middleman, S., 1967. Drop size distribution in agitated liquid-liquid systems. *AIChE J.* 13, 989–995. doi:10.1002/aic.690130529
- Coulaloglou, C.A., Tavlarides, L.L., 1977. Description of interaction processes in agitated liquid-liquid dispersions. *Chem. Eng. Sci.* 32, 1289–1297. doi:10.1016/0009-2509(77)85023-9
- Coulaloglou, C. a., Tavlarides, L.L., 1976. Drop Size Distributions and Coalescence Frequencies of Liquid-Liquid Dispersions in Flow Vessels. *AIChE J.* 22, 289–297. doi:10.1002/aic.690220211
- Crowe, C.T., Schwarzkopf, J.D., Sommerfeld, M., Tsuji, Y., 2011. *Multiphase Flows with Droplets and Particles*, Second Edition.
- Farzad, R., Puttering, S., Pirker, S., Schneiderbauer, S., 2016. Experimental investigation of liquid-liquid system drop size distribution in Taylor-Couette flow and its application in the CFD simulation. *Proc. Exp. Fluid Mech.* 2016 Conf. Lázně, Czech Repub.
- Kolmogorov, a N., 1941. The local structure of turbulence in incompressible viscous fluid for very large Reynolds numbers. *Dokl. Akad. Nauk Sssr* 30, 301–305. doi:10.1098/rspa.1991.0075
- Leng, D.E., Calabrese, R. V., 2004. Immiscible Liquid-Liquid Systems, in: Paul, E.L., Atiemo-Obeng, V.A., Kresta, S.M. (Eds.), *Handbook of Industrial Mixing*. John Wiley & Sons, Inc., pp. 639–753. doi:10.1002/0471451452.ch12
- Maaß, S., Gäbler, A., Zaccone, A., Paschedag, A.R., Kraume, M., 2007. Experimental Investigations and Modelling of Breakage Phenomena in Stirred Liquid/Liquid Systems. *Chem. Eng. Res. Des.* 85, 703–709. doi:10.1205/cherd06187
- Maaß, S., Paul, N., Kraume, M., 2012. Influence of the dispersed phase fraction on experimental and predicted drop size distributions in breakage dominated stirred systems. *Chem. Eng. Sci.* 76, 140–153. doi:10.1016/j.ces.2012.03.050
- Narsimhan, G., Ramkrishna, D., Gupta, J.P., 1980. Analysis of drop size distributions in lean liquid-liquid dispersions. *AIChE J.* 26, 991–1000. doi:10.1002/aic.690260614
- Ohtake, T., Hano, T., Takagi, K., Nakashio, F., 1987. Effects of Viscosity on Drop Diameter of W/O Emulsion Dispersed in a Stirred Tank. *J. Chem. Eng. Japan* 20, 443–447. doi:10.1252/jcej.20.443
- Ramkrishna, D., 2000. *Population Balances*, Chemical Engineering.
- Ranade, V. V., 2001. *Computational Flow Modeling for Chemical Reactor Engineering*.
- Roudsari, S.F., Turcotte, G., Dhib, R., Ein-Mozaffari, F., 2012. CFD modeling of the mixing of water in oil emulsions. *Comput. Chem. Eng.* 45, 124–136. doi:10.1016/j.compchemeng.2012.06.013
- Schellander, D., Schneiderbauer, S., Pirker, S., 2012. Numerical study of agglomeration modeling in polydispersed gas-solid flows with respect to particle separation. *Ninth Int. Conf. CFD Miner. Process Ind.* CSIRO, Melbourne, Aust.
- Schneiderbauer, S., Haider, M.F., Hauzenberger, F., Pirker, S., 2016a. A Lagrangian-Eulerian hybrid model for the simulation of industrial-scale gas-solid cyclones. *Powder Technol.* 304, 229–240. doi:10.1016/j.powtec.2016.07.064
- Schneiderbauer, S., Pirker, S., Puttering, S., Aguayo, P., Touloupidis, V., Joaristi, A.M., 2016b. A Lagrangian-Eulerian hybrid model for the simulation of poly-disperse fluidized beds: Application to industrial-scale olefin polymerization. *Powder Technol.* In Press. doi:10.1016/j.powtec.2016.12.063
- Schneiderbauer, S., Puttering, S., Pirker, S., Aguayo, P., Kanellopoulos, V., 2015. CFD modeling and simulation of industrial scale olefin polymerization fluidized bed reactors. *Chem. Eng. J.* 264, 99–112.
- Shinnar, R., Church, J.M., 1960. Statistical Theories of Turbulence in Predicting Particle Size in Agitated Dispersions. *Ind. Eng. Chem.* 52, 253–256. doi:10.1021/ie50603a036
- Solsvik, J., Becker, P.J., Sheibat-Othman, N., Mohallick, I., Farzad, R., Jakobsen, H.A., 2014. Viscous Drop Breakage in Liquid-Liquid Stirred Dispersions: Population Balance Modeling. *J. Dispers. Sci. Technol.* 36, 577–594.
- Solsvik, J., Jakobsen, H.A., 2015. Single drop breakup experiments in stirred liquid-liquid tank. *Chem. Eng. Sci.* 131, 219–234. doi:10.1016/j.ces.2015.03.059
- Wang, C.Y., Calabrese, R. V., 1986. Drop breakup in turbulent stirred-tank contactors. Part II: Relative influence of viscosity and interfacial tension. *AIChE J.* 32, 667–676. doi:10.1002/aic.690320417